The 9th European Congress on Computational Methods in Applied Sciences and Engineering
ECCOMAS Congress 2024
3–7 June 2024, Lisboa, Portugal

RECENT ADVANCES IN THE POSTBUCKLING ANALYSIS OF COMPOSITE LAMINATED STRUCTURES

Francesco S. Liguori[1], Giovanni Zucco[2], and Antonio Madeo[1]

[1] University of Calabria
DIMES, Ponte P. Bucci, Cubo 42 B
87036 Rende (Cosenza), Italy
e-mail: francesco.liguori@unical.it and antonio.madeo81@unical.it

[2] University of Limerick
School of Engineering and Bernal Institute
Limerick, Ireland
e-mail: giovanni.zucco@ul.ie

Key words: Geometrically nonlinear analysis, FEM, Thin-walled structures, Composite laminates

Summary. The current demand for lightweight structures in a wide range of engineering applications leads to using thin-walled composite laminated structures whose behaviour is governed by buckling and postbuckling phenomena. Such a demand is pushing the borders of computational mechanics to enhance methods and algorithms for studying those structures' geometrically nonlinear responses. This work presents some of the authors' developments in analysing lightweight composite laminated structures. The literature survey introduces a family of finite elements known as MISS elements, where MISS stands for mixed isostatic self-equilibrated stresses. The description of those elements, which are derived from the Hellinger-Reissner functional, is followed by a discussion on their advantages concerning displacement-based elements when studying composite laminated thin-walled structures. Subsequently, a framework for the postbuckling analysis of composite structures with the MISS-4C element that uses the Koiter multi-modal approach is presented.

1 INTRODUCTION

Composite shell structures undergoing large deformations are used in various civil, mechanical and aerospace engineering applications. Several design strategies have been developed to exploit the potential that composite laminates offer to reduce the weight of those structures and enhance their carrying load capacity [19, 11, 7]. When large deformations are involved, the efficiency and robustness of geometrically nonlinear analysis tools play a crucial aspect in the analysis and design of composite laminated thin-walled structures. In this regard, appealing strategy solutions are represented by those using mixed Finite Element (FE) formulations that assume both displacement and stress fields as primary variables [6, 20].

In those elements, the functions interpolating the stress fields must be accurately chosen to avoid spurious energy modes. In 2015, Madeo et al. [17] presented a mixed element, derived from the Hellinger-Reissner functional, whose stress fields a priori satisfy the equilibrium equations for zero bulk loads. Furthermore, that element was formulated to be isostatic namely its number

of kinematic Degrees Of Freedom (DOFs) equals the number of parameters used in the functions interpolating its stress fields. As such, the element was named MISS-4 standing for Mixed Isostatic Self equilibrating Stress-4 nodes. MISS-4 showed good convergence properties when used for solving linear elastic static shell problems. Subsequently, MISS-4 was used for solving linear buckling [3, 22] and initial post-buckling [2, 14] problems of composite laminated thin-walled structures with constant and variable stiffness showing good convergence properties and robustness. The efficiency of MISS-4 when used within a Koiter multi-modal approach to study the initial post-buckling behaviour of slender structures was then exploited to develop a fast tool for studying the imperfection sensitivity analysis of those structures subjected to initial geometrical imperfections [4, 9, 1].

A successful strategy to further enhance the performance of mixed elements is the Trefftz method, which uses assumed stresses that a-priori satisfy both equilibrium equations for zero bulk loads and compatibility equations in the linear-elastic case [5, 8]. Exploiting the Trefftz method, Madeo et al. [15] developed a mixed 8-nodes for the linear-elastic analysis of isotropic shell structures, named MISS-8. This element showed high accuracy and convergence rate when used for discretising structures with coarse meshes, and insensitivity to mesh distortions. However, developing Trefftz FE to study composite laminated structures is not straightforward because the matrix of the elastic coefficients has influence on the compatibility equations and, therefore, on the interpolation of the stress fields. In this regard, the family of MISS element was then extended to MISS-4C which is developed through the hybrid-Trefftz method so that its stress fields a priori satisfy both the equilibrium for zero bulk loads and the compatibility equations [13]. More precisely, MISS-4C uses stress fields that are bespoke for composite laminated thin-walled structures with symmetric layups. Its geometry is flat and has 24 DOFs to describe its kinematics, located at its four vertices, namely each node has three three translations and three rotations, including drilling. The element is isostatic and, therefore, the number of stress parameters is 18.

Another appealing discretisation method for studying the postbuckling response of composite laminated slender structures is represented by solid-shell elements whose kinematics is described only through translations [18, 12]. In fact, starting from a three-dimensional description at the continuum level, solid-shell models are developed by interpolating the displacements along the thickness of the shell, resulting in generalised strain and stress fields that depend on the midplane coordinates [21].

Similarly to the mixed shell element mentioned above, also solid-shell elements can be further enhanced exploiting the Trefftz method [5]. In this regard, recently Liguori et al. [10] proposed a mixed solid-shell hexahedral element for the geometrically nonlinear analysis of isotropic elastic shells whose name is MISS-4S, which stands for Mixed Isostatic Self equilibrating Stresses, 4-nodes, Solid-shell. The element has six translational DOFs at each vertex of the solid-shall mid-plane and is implemented within a path-following strategy that uses the Riks method to solve geometrically nonlinear problems.

This work briefly recalls the theory of MISS-4C for studying the postbuckling analysis of composite laminated thin-walled structures. Whereas the description of MISS4-S for studying those problems with a solid-shell element can be found in companion work presented in this conference [10].

2 THEORY

This Section presents a brief recall of the theory beyond the development of MISS4-C, while its details can be found in [13].

2.1 LINEAR FORMULATION

MISS-4C has four nodes located at its vertex and a quadrilateral. Each node has three translations and three rotations for a total of 24 DOFs. The generalised stresses are interpolated to be isostatic [16], namely the number of stress parameters n_β equals the number of DOFs describing the kinematic minus the number of rigid body motions $n_r = 6$, i.e. $n_\beta = n_d - n_r = 18$. Furthermore, the stress interpolation functions satisfy both the equilibrium equations for zero bulk loads (Eq. (**??**)) and the compatibility equations (Eq. (**??**)). As such, the element's displacement field is assumed only along its contour [8].

2.1.1 Geometry and reference systems

A global Cartesian system $\{X,\, Y,\, Z\}$ defines the position of the element in the three-dimensional space and is defined so that the nodes lay on the plane $\{X,\, Y\}$. Then, a dimensionless internal system $\{\xi,\, \eta\}$ is defined over the element mid-surface with $-1 \leq \xi \leq 1, -1 \leq \eta \leq 1$. Finally, a local Cartesian system $\{x,\, y\}$ is centred and aligned so as to reduce the element distortion.

The internal system $\{\xi,\, \eta\}$ can be indirectly defined as

$$\begin{cases} X = A_0 + A_1\xi + A_2\xi\eta + A_3\eta \\ Y = B_0 + B_1\xi + B_2\xi\eta + B_3\eta \end{cases} , \quad \begin{bmatrix} A_0 & B_0 \\ A_1 & B_1 \\ A_2 & B_2 \\ A_3 & B_3 \end{bmatrix} = \frac{1}{4} \begin{bmatrix} 1 & 1 & 1 & 1 \\ -1 & 1 & 1 & -1 \\ 1 & -1 & 1 & -1 \\ -1 & -1 & 1 & 1 \end{bmatrix} \begin{bmatrix} X_1 & Y_1 \\ X_2 & Y_2 \\ X_3 & Y_3 \\ X_4 & Y_4 \end{bmatrix} , \tag{1}$$

where $\{X_i,\, Y_i\}$, $i = 1, \ldots, 4$, are the nodal coordinates in the global system $\{X,\, Y,\, Z\}$. To define the local Cartesian system $\{x, y\}$, a Jacobian matrix $\boldsymbol{J}_G$ is introduced

$$\boldsymbol{J}_G = \begin{bmatrix} X_{,\xi} & X_{,\eta} \\ Y_{,\xi} & Y_{,\eta} \end{bmatrix} = \begin{bmatrix} (A_1 + A_2\eta) & (A_3 + A_2\xi) \\ (B_1 + B_2\eta) & (B_3 + B_2\xi) \end{bmatrix} . \tag{2}$$

An average Jacobian $\bar{\boldsymbol{J}}^G$ is evaluated as

$$\bar{\boldsymbol{J}}_G = \frac{1}{4} \int_{-1}^{1} \int_{-1}^{1} \boldsymbol{J}_G \, \mathrm{d}\xi \, \mathrm{d}\eta = \begin{bmatrix} A_1 & A_3 \\ B_1 & B_3 \end{bmatrix} , \tag{3}$$

which is decomposed into an orthogonal matrix $\boldsymbol{R}$ and a symmetric matrix $\bar{\boldsymbol{J}}$ as

$$\bar{\boldsymbol{J}}^G = \boldsymbol{R}\,\bar{\boldsymbol{J}} \quad , \quad \begin{cases} \boldsymbol{R} = \begin{bmatrix} \cos\alpha & -\sin\alpha \\ \sin\alpha & \cos\alpha \end{bmatrix} , \quad \alpha = \arctan\left(\dfrac{A_3 - B_1}{A_1 + B_3}\right) \\ \bar{\boldsymbol{J}} = \begin{bmatrix} a & c \\ c & b \end{bmatrix} = \boldsymbol{R}^T \bar{\boldsymbol{J}}_G \end{cases} . \tag{4}$$

The local Cartesian system $\{x, y\}$ has its origin coincident with the element centroid ($\xi = \eta = 0$) and is rigidly rotated through $\boldsymbol{R}$ with respect to $\{X, Y\}$.

The following expression defines the $\{x, y\}$ coordinates

$$\begin{bmatrix} x \\ y \end{bmatrix} = \boldsymbol{R}^T \begin{bmatrix} X - A_0 \\ Y - B_0 \end{bmatrix}. \tag{5}$$

Finally, for each element' side, Γ_k, which connects the nodes i and j in anticlockwise sense, the following quantities are introduced

$$\boldsymbol{g}_k = \begin{bmatrix} g_{kx} \\ g_{ky} \end{bmatrix} = \begin{bmatrix} x_j + x_i \\ y_j + y_i \end{bmatrix} \quad , \quad \bar{\boldsymbol{g}}_k = \begin{bmatrix} \bar{g}_{kx} \\ \bar{g}_{ky} \end{bmatrix} = \begin{bmatrix} x_j - x_i \\ y_j - y_i \end{bmatrix} \quad , \quad \boldsymbol{n}_k = \begin{bmatrix} n_x \\ n_y \end{bmatrix} = \frac{1}{L_k} \begin{bmatrix} d_{ky} \\ -d_{kx} \end{bmatrix} \tag{6}$$

where $L_k = \sqrt{\bar{g}_{kx}^2 + \bar{g}_{ky}^2}$ is the side length, while $\boldsymbol{n}_k$ is the external normal to Γ_k. In the following part, the one-dimensional abscissa $-1 \leq \zeta \leq 1$ along Γ_k is used so that

$$x = \frac{1}{2}(g_{kx} + \bar{g}_{kx}\,\zeta), \quad y = \frac{1}{2}(g_{ky} + \bar{g}_{ky}\,\zeta). \tag{7}$$

2.2 Generalised stress field interpolation

The assumed interpolation for the generalised stresses is chosen so as to satisfy equilibrium equations for zero bulk loads and compatibility equations. Additionally, they are isostatic and then $n_\beta = 18$. The membrane and flexural generalised stress fields are interpolated separately and ruled by 9 static parameters each. Moreover, the generalised stresses are defined in the local system $\{x,\, y\,\}$.

2.2.1 Assumed in-plane stress field

The in-plane stress field is interpolated through $\boldsymbol{d}_{tm}$ defined as

$$\boldsymbol{d}_{tm} = \bar{\boldsymbol{B}}_m \bar{\boldsymbol{\beta}}_m \quad , \quad \bar{\boldsymbol{B}}_m = \begin{bmatrix} \bar{\boldsymbol{B}}_{mu} & \cdot \\ \cdot & \bar{\boldsymbol{B}}_{mu} \end{bmatrix}, \tag{8}$$

where

$$\bar{\boldsymbol{B}}_{mu} = \begin{bmatrix} 1 & x & y & x^2 & xy & y^2 & \cdots & x^4 & x^3y & x^2y^2 & xy^3 & y^4 \end{bmatrix} \tag{9}$$

and $\bar{\boldsymbol{\beta}}_m$ is a $[30 \times 1]$ vector. By applying the compatibility and constitutive equations for the case of symmetric composite laminates to Eq. (8), the generalised in-plane stress field becomes

$$\boldsymbol{t}_m = \boldsymbol{E}_m \boldsymbol{Q}_m \bar{\boldsymbol{B}}_m \bar{\boldsymbol{\beta}}_m. \tag{10}$$

Then, that field is rewritten by superimposing the equilibrium and a hierarchical selection of nine independent polynomials is conducted leading to

$$\boldsymbol{t}_m = \boldsymbol{B}_m \boldsymbol{\beta}_m, \tag{11}$$

where $\boldsymbol{B}_m$ is matrix depending on the coefficients $E_{ij}, i, j = 1..8$ of the matrix, $\mathbf{E}$ collecting the elastic coefficients for composite laminates using the First Order Shear Deformation Theory.

The expression of $\boldsymbol{B}_m$ can be found in [13], while for a simple case as when $E_{13} = E_{23} = 0$ it becomes

$$\boldsymbol{B}_m = \left[\begin{array}{ccc|cccc|cc} E_{11} & E_{12} & 0 & 0 & -x & y & 0 & -2\,x\,y & E_{11}\,y^2 \\ E_{21} & E_{22} & 0 & x & 0 & 0 & y & 2\,x\,y & -E_{22}\,x^2 \\ \underbrace{0} & \underbrace{0} & \underbrace{E_{33}} & \underbrace{0} & \underbrace{y} & \underbrace{0} & \underbrace{-x} & \underbrace{y^2 - x^2} & \underbrace{0} \\ \multicolumn{3}{c}{\text{cost}} & \multicolumn{4}{c}{\text{lin}} & \multicolumn{2}{c}{\text{quad}} \end{array}\right] \tag{12}$$

It is worth noting from Eq. (12) that the in-plane stress interpolation, satisfying equilibrium and compatibility equations, varies according to the material coefficients and lamination stacking sequence.

Finally, the membrane part of the elastic displacement solution $\boldsymbol{d}_{tm}$ is expressed in terms of static parameters $\boldsymbol{\beta}_m$ as

$$\boldsymbol{d}_{tm} = \boldsymbol{D}_{tm}\boldsymbol{\beta}_m, \tag{13}$$

where

$$\boldsymbol{D}_{tm} = \left[\begin{array}{c|c|c} \boldsymbol{D}_{tm}^{(0)} & \boldsymbol{D}_{tm}^{(1)} & \boldsymbol{D}_{tm}^{(2)} \end{array}\right], \tag{14}$$

and the expressions of $\boldsymbol{D}_{tm}^{(0)}, \boldsymbol{D}_{tm}^{(1)}, \boldsymbol{D}_{tm}^{(2)}$ are given in [13].

2.2.2 Assumed flexural stress field

The flexural stress field interpolation, $\boldsymbol{d}_{tf}$, is assumed as

$$\boldsymbol{d}_{tf} = \bar{\boldsymbol{B}}_f\bar{\boldsymbol{\beta}}_f \quad , \quad \bar{\boldsymbol{B}}_f = \left[\begin{array}{ccc} \bar{\boldsymbol{B}}_{fu} & \cdot & \cdot \\ \cdot & \bar{\boldsymbol{B}}_{f\varphi} & \cdot \\ \cdot & \cdot & \bar{\boldsymbol{B}}_{f\varphi} \end{array}\right], \tag{15}$$

where

$$\begin{aligned} \bar{\boldsymbol{B}}_{fu} &= \left[\begin{array}{cccccccccccc} 1 & x & y & x^2 & xy & y^2 & \cdots & x^5 & x^4y & x^3y^2 & x^2y^3 & xy^4 & y^5 \end{array}\right], \\ \bar{\boldsymbol{B}}_{f\varphi} &= \left[\begin{array}{cccccccccccc} 1 & x & y & x^2 & xy & y^2 & \cdots & x^4 & x^3y & x^2y^2 & xy^3 & y^4 \end{array}\right] \end{aligned} \tag{16}$$

while $\bar{\boldsymbol{\beta}}_f$ is a $[51 \times 1]$ vector. By applying the compatibility and constitutive equations for symmetric composite laminates to Eq. (15), $\boldsymbol{t}_f$ becomes

$$\boldsymbol{t}_f = \boldsymbol{E}_f\boldsymbol{Q}_f\bar{\boldsymbol{B}}_f\bar{\boldsymbol{\beta}}_f. \tag{17}$$

Subsequently, $\boldsymbol{t}_f$ is rewritten by superimposing the equilibrium and a hierarchical selection of nine independent polynomials as

$$\boldsymbol{t}_f = \boldsymbol{B}_f\boldsymbol{\beta}_f, \tag{18}$$

where $\boldsymbol{\beta}_f$ is a $[9 \times 1]$ vector while $\boldsymbol{B}_f$ is a matrix depending on $\mathbf{E}$ whose terms can be found in [13].

The hierarchical selection of the assumed stress interpolation is obtained by including the lowest-order polynomial shapes that satisfy the isostatic condition and that avoid spurious energy modes. Similarly to the interpolation of the in-plane stress fields, the interpolation of the flexural stresses, satisfying equilibrium and compatibility, depends on the material properties and stacking sequence of the composite laminate.

Finally, the flexural part of the elastic displacement field $\boldsymbol{d}_{tf}$ is rewritten as a function of the static parameters $\boldsymbol{\beta}_f$ as

$$\boldsymbol{d}_{tf} = \boldsymbol{D}_{tf}\boldsymbol{\beta}_f, \tag{19}$$

where

$$\boldsymbol{D}_{tf} = \left[\begin{array}{c|c|c} \boldsymbol{D}_{tf}^{(0)} & \boldsymbol{D}_{tf}^{(1)} & \boldsymbol{D}_{tf}^{(2)} \end{array} \right]. \tag{20}$$

The expressions of $\boldsymbol{D}_{tf}^{(0)}, \boldsymbol{D}_{tf}^{(1)}, \boldsymbol{D}_{tf}^{(2)}$ can be found in [13].

2.3 Generalised displacement field interpolation

The interpolation of the displacement field $\boldsymbol{d}$ is ruled by 24 nodal translation and rotations, collected in the vector $\boldsymbol{d}_e$.

Due to the assumptions on the generalised stress field (see Section (2.2)), the displacement field is interpolated only along the contour of MISS4-C. As such, for a generic side Γ_k having end nodes i, j, the displacement parameters are collected in the vectors $\boldsymbol{d}_{ie} = [d_{ix},\, d_{iy},\, d_{iz},\, \varphi_{ix},\, \varphi_{iy},\, \varphi_{iz}]^T$ and $\boldsymbol{d}_{je} = [d_{jx},\, d_{jy},\, d_{jz},\, \varphi_{jx},\, \varphi_{jy},\, \varphi_{jz}]^T$, respectively.

2.4 Assumed in-plane displacement field

The membrane displacements along the generic side Γ_k are defined as the sum of three contributions

$$\boldsymbol{d}_{km}[\zeta] = \boldsymbol{d}_{km}^{(l)}[\zeta] + \boldsymbol{d}_{km}^{(q)}[\zeta] + \boldsymbol{d}_{km}^{(c)}[\zeta], \tag{21a}$$

where ζ is the one-dimensional abscissa $-1 \leq \zeta \leq 1$ along Γ_k (see Eq. (7)). The first contribution in Eq. (21a) is a linear interpolation from the vertex values

$$\boldsymbol{d}_{km}^{(l)}[\zeta] = \frac{1}{2}[(1-\zeta)\,\boldsymbol{d}_i + (1+\zeta)\,\boldsymbol{d}_j]\,, \quad \boldsymbol{d}_i = [d_{ix},\, d_{iy}]^T\,, \quad \boldsymbol{d}_j = [d_{jx},\, d_{jy}]^T. \tag{21b}$$

The second contribution is a quadratic expansion for the normal displacement

$$\boldsymbol{d}_{km}^{(q)}[\zeta] = \frac{L_k}{8}\,(1-\zeta^2)(\varphi_{jz} - \varphi_{iz})\,\boldsymbol{n}_k \tag{21c}$$

evaluated according to Allman's kinematic [16] the third contribution is a cubic expansion for the normal component of the side displacement defined as

$$\boldsymbol{d}_{km}^{(c)}[\zeta] = \frac{1}{4}\,L_k(\zeta - \zeta^3)\boldsymbol{n}_k\,\alpha_c, \tag{21d}$$

where α_c is the average distortional drilling nodal rotation obtained as

$$\alpha_c = \frac{1}{4}\sum_{i=1}^{4} \varphi_{iz} - \varphi_{ez} \tag{21e}$$

$$\varphi_{ez} = \boldsymbol{N}_\varphi \boldsymbol{d}_{me} \tag{21f}$$

$$\boldsymbol{N}_\varphi = \frac{1}{4\Omega_e}\,[-y_4 + y_3,\; x_4 - x_3, 0,\; -y_4 + y_1,\; x_4 - x_1, 0,\; -y_2 + y_1,\; x_2 - x_1, 0,\; -y_3 + y_2,\; x_3 - x_2, 0]$$

where Ω_e is the area of finite element and $\boldsymbol{d}_{me}$ is a $[12\times1]$ vector collecting the in-plane kinematic parameters defined as

$$\boldsymbol{d}_{me} = [d_{1x}, d_{1y}, \varphi_{1z} \cdots d_{4x}, d_{4y}, \varphi_{4z}]^T. \tag{21g}$$

Equations (21) are rewritten as

$$\boldsymbol{d}_{km}[\zeta] = \boldsymbol{D}_{km}[\zeta]\boldsymbol{d}_{me}\ , \quad \boldsymbol{D}_{km}[\zeta] = \boldsymbol{D}^{(l)}_{km}[\zeta] + \boldsymbol{D}^{(q)}_{km}[\zeta] + \boldsymbol{D}^{(c)}_{km}[\zeta]. \tag{22}$$

It is worth noting that the linear $\boldsymbol{d}^{(l)}_{km}$ and quadratic $\boldsymbol{d}^{(q)}_{km}$ parts of the in-plane displacement field are continuous at the inter-element boundaries. Whereas the cubic contribution $\boldsymbol{d}^{(c)}_{km}$ corresponds to an incompatible mode, which is orthogonal on average to a constant and linear stress and prevents rank defectiveness of the element [16].

2.5 Assumed flexural displacement field

The displacement $u_{kz}[\zeta]$ along Γ_k is assumed as the sum of a linear, a quadratic and a cubic contribution, namely

$$d_{kz}[\zeta] = d^{(l)}_{kz}[\zeta] + d^{(q)}_{kz}[\zeta] + d^{(c)}_{kz}[\zeta] \quad , \quad \begin{cases} d^{(l)}_{kz}[\zeta] = \dfrac{1}{2}\left[(1-\zeta)d_{iz} + (1+\zeta)d_{jz}\right] \\ d^{(q)}_{kz}[\zeta] = \dfrac{L_k}{8}\,(1-\zeta^2)(\boldsymbol{\varphi}_{ki} - \boldsymbol{\varphi}_{kj})^T\boldsymbol{n}_k\ , \\ d^{(c)}_{kz}[\zeta] = -\dfrac{L_k}{4}\left(\zeta^3 - \zeta\right)\varphi_{en} \end{cases} \tag{23a}$$

where

$$\boldsymbol{\varphi}_{ki} = [\varphi_{ix}, \varphi_{ix}]^T \quad , \quad \boldsymbol{\varphi}_{kj} = [\varphi_{jx}, \varphi_{jy}]^T \quad , \quad \varphi_{en} = \frac{1}{8}\sum_{k=1}^{4}\left(\boldsymbol{\varphi}_{kj} - \boldsymbol{\varphi}_{ki}\right)^T\boldsymbol{n}_k - \frac{1}{2}(\varphi_{ex}+\varphi_{ey}) \tag{23b}$$

and

$$\varphi_{ex} = \frac{1}{2}\left(\left(d_{4z} - d_{1z}\right)/L_4 + \left(d_{3z} - d_{2z}\right)/L_2\right) \quad , \quad \varphi_{ey} = \frac{1}{2}\left(\left(d_{4z} - d_{3z}\right)/L_3 + \left(d_{1z} - d_{2z}\right)/L_1\right). \tag{23c}$$

The normal rotation $\varphi_{kn}[\zeta]$ along Γ_k is assumed to be the sum of a linear and a quadratic contribution

$$\varphi_{kn}[\zeta] = \varphi^{(l)}_{kn}[\zeta] + \varphi^{(q)}_{kn}[\zeta] \quad , \quad \begin{cases} \varphi^{(l)}_{kn}[\zeta] = \dfrac{1}{2}\left[(1-\zeta)\varphi_{in} + (1+\zeta)\varphi_{jn}\right] \\ \varphi^{(q)}_{kn}[\zeta] = 2\,d^{(c)}_{kz}[\zeta]_{,\zeta}/L_k \end{cases} \tag{23d}$$

Similarly, the tangential rotation $\varphi_{kt}[\zeta]$ is assumed as

$$\varphi_{kt}[\zeta] = \varphi^{(l)}_{kt}[\zeta] \quad , \quad \varphi^{(l)}_{kt}[\zeta] = \frac{1}{2}\left[(1-\zeta)\varphi_{it} + (1+\zeta)\varphi_{jt}\right]. \tag{23e}$$

By introducing the following relationships between rotations

$$\begin{bmatrix}\varphi_{kx}[\zeta] \\ \varphi_{ky}[\zeta]\end{bmatrix} = \begin{bmatrix} n_x & -n_y \\ n_y & n_x\end{bmatrix}\begin{bmatrix}\varphi_{kn}[\zeta] \\ \varphi_{kt}[\zeta]\end{bmatrix} \tag{23f}$$

and

$$\begin{cases} \varphi_{in} = n_x\,\varphi_{ix} + n_y\,\varphi_{iy} \\ \varphi_{it} = n_x\,\varphi_{iy} - n_y\,\varphi_{ix} \end{cases} \quad , \quad \begin{cases} \varphi_{jn} = n_x\,\varphi_{jx} + n_y\,\varphi_{jy} \\ \varphi_{jt} = n_x\,\varphi_{jy} - n_y\,\varphi_{jx} \end{cases}, \tag{23g}$$

the $[12 \times 1]$ vector collecting the out-of-plane kinematic parameters is

$$\boldsymbol{d}_{fe} = [d_{1z}, \varphi_{1x}, \varphi_{1y}, \cdots d_{4z}, \varphi_{4x}, \varphi_{4y}]^T. \tag{23h}$$

Equations (23) are rewritten as

$$\boldsymbol{d}_{kf}[\zeta] = \begin{bmatrix} d_{kz}[\zeta] \\ \varphi_{kx}[\zeta] \\ \varphi_{ky}[\zeta] \end{bmatrix} = \boldsymbol{D}_{kf}[\zeta]\boldsymbol{d}_{fe}\ , \quad \boldsymbol{D}_{kf}[\zeta] = \boldsymbol{D}_{kf}^{(l)}[\zeta] + \boldsymbol{D}_{kf}^{(q)}[\zeta] + \boldsymbol{D}_{kf}^{(c)}[\zeta]. \tag{24}$$

2.6 Compliance and compatibility element operators

On the basis of the assumed stress and displacement field interpolations, the compatibility matrix, $\boldsymbol{Q}_e$ and the element compliance matrix, $\boldsymbol{H}_e$ of the single element, e, are

$$\boldsymbol{Q}_e = \begin{bmatrix} \boldsymbol{Q}_m & \cdot \\ \cdot & \boldsymbol{Q}_f \end{bmatrix} \quad , \quad \begin{cases} \boldsymbol{Q}_m = \displaystyle\int_{\Omega_e} \left\{ \boldsymbol{B}_m^T \boldsymbol{Q}_m \boldsymbol{D}_m \right\} \mathrm{d}\Omega \\ \boldsymbol{Q}_f = \displaystyle\int_{\Omega_e} \left\{ \boldsymbol{B}_f^T \boldsymbol{Q}_f \boldsymbol{D}_f \right\} \mathrm{d}\Omega \end{cases}, \tag{25a}$$

and

$$\boldsymbol{H}_e = \begin{bmatrix} \boldsymbol{H}_m & \cdot \\ \cdot & \boldsymbol{H}_f \end{bmatrix} \quad , \quad \begin{cases} \boldsymbol{H}_m = \displaystyle\int_{\Omega_e} \left\{ \boldsymbol{B}_m^T \boldsymbol{E}_m^{-1} \boldsymbol{B}_m \right\} \mathrm{d}\Omega \\ \boldsymbol{H}_f = \displaystyle\int_{\Omega_e} \left\{ \boldsymbol{B}_f^T \boldsymbol{E}_f^{-1} \boldsymbol{B}_f \right\} \mathrm{d}\Omega \end{cases}, \tag{25b}$$

where the matrices $\boldsymbol{Q}_m$ and $\boldsymbol{H}_m$ collect the in-plane contributions of $\boldsymbol{Q}_e$ and $\boldsymbol{H}_e$, respectively. Similarly, the flexural contributions are collected in $\boldsymbol{Q}_f$ and $\boldsymbol{H}_f$, respectively. Both the compatibility and compliance element matrices are evaluated through a line integration along the element contour as

$$\boldsymbol{Q}_m = \sum_{k=1}^{4} \boldsymbol{Q}_{km} \quad , \quad \boldsymbol{Q}_f = \sum_{k=1}^{4} \boldsymbol{Q}_{kf} \quad , \quad \boldsymbol{H}_m = \sum_{k=1}^{4} \boldsymbol{H}_{km} \quad , \quad \boldsymbol{H}_f = \sum_{k=1}^{4} \boldsymbol{H}_{kf}, \tag{25c}$$

with $\boldsymbol{Q}_{km}$ and $\boldsymbol{Q}_{kf}$ defined as

$$\boldsymbol{Q}_{km} = \int_{-1}^{1} \boldsymbol{B}_m^T[\zeta] \boldsymbol{N}_{km} \boldsymbol{D}_{km}[\zeta]\, \mathrm{d}\zeta \quad , \quad \boldsymbol{Q}_{kf} = \int_{-1}^{1} \boldsymbol{B}_f^T[\zeta] \boldsymbol{N}_{kf} \boldsymbol{D}_{kf}[\zeta]\, \mathrm{d}\zeta, \tag{25d}$$

while $\boldsymbol{H}_{km}$ and $\boldsymbol{H}_{kf}$ are

$$\boldsymbol{H}_{km} = \int_{-1}^{1} \boldsymbol{B}_m^T[\zeta] \boldsymbol{N}_{km} \boldsymbol{D}_{ktm}[\zeta]\, \mathrm{d}\zeta \quad , \quad \boldsymbol{H}_{kf} = \int_{-1}^{1} \boldsymbol{B}_f^T[\zeta] \boldsymbol{N}_{kf} \boldsymbol{D}_{ktf}[\zeta]\, \mathrm{d}\zeta. \tag{25e}$$

The matrices $\boldsymbol{N}_{km}$ and $\boldsymbol{N}_{kf}$ collect the components of the normal vector to Γ_k to define the projections of stresses and displacements, respectively . Finally, $\boldsymbol{D}_{ktm}[\zeta]$ and $\boldsymbol{D}_{ktf}[\zeta]$ represent the evaluation along Γ_k of the matrices defined in Eqs. (14) and (20), respectively.

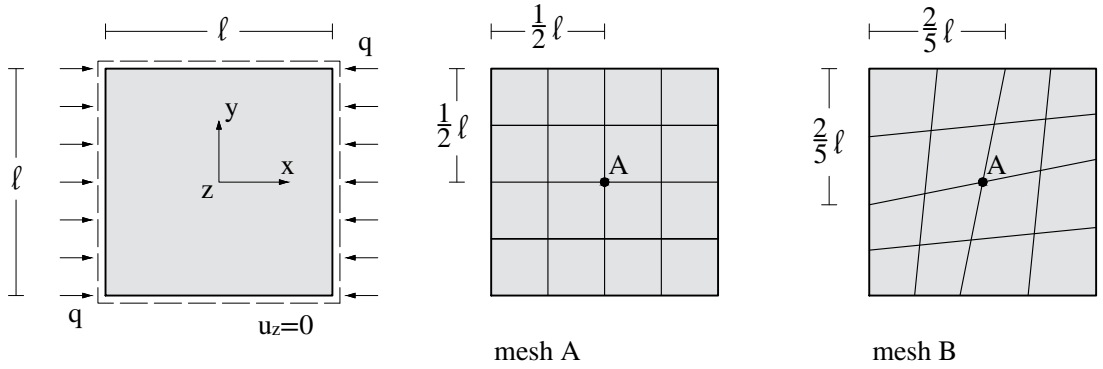

Figure 1: Composite laminated square plate: geometry, loads, boundary conditions and initial meshes.

2.7 Postbuckling analysis

A corotational approach is used to employ the linear static formulation of MISS-4C to solve geometrically nonlinear problems. In particular, this work uses a reduced-order model based on Koiter's theory to obtain an asymptotic approximation solution of the initial postbuckling behaviour of composite laminated thin-walled structures [14]. The number of buckling modes included in the construction of the reduced order model is usually a few tens. A discussion on how buckling modes contribute to the nonlinear solution has been recently presented by Zucco and Weaver [24], who identified a strategy to further reduce the computational cost of that analysis by taking into account the degree of symmetry of the structure under consideration.

3 NUMERICAL RESULTS

This Section investigates the performance of MISS-4C through the postbuckling analysis of a composite laminated plate under compressive loading.

3.1 Composite laminated plate under compressive loading

The test regards a composite square plate under compression loading whose geometry, loading and boundary conditions are shown in Fig. 1. The length of the plate is $\ell = 0.508$, while its thickness equals $1.172 \cdot 10^{-4}$. The plate is simply supported (SS1) and in-plane constraints are used to prevent rigid body motions. A compression load $q_x = 1$ is uniformly distributed along both plate's vertical sides. Furthermore, a uniformly distributed out-of-plane load $q_z = 10^{-8}$ is applied. A regular and a distorted mesh are considered, as shown in Fig. 1. The material properties are $E_{11} = 181 \cdot 10^3$, $E_{22} = 10.27 \cdot 10^3$, $G_{12} = 7.17 \cdot 10^3$, $G_{13} = G_{23} = 5.135 \cdot 10^6$ and $\nu_{12} = 0.28$. The material directions 1 and 2 are aligned with the $x-$ and $y-$axis, respectively. The laminate stacking sequence is $[\pm 45]_{2S}$.

Table 1 shows the four lowest buckling loads for different mesh refinements obtained with MISS-4C, MISS-4, and S8 R in Abaqus. It is worth noting that results obtained with MISS-4C have a better accuracy than those obtained with MISS-4. For all the buckling loads in Table 1 both MISS-4 and MISS-4C exhibit a rate of convergence of h^2. However, MISS-4C gives a lower error in the evaluation of the first buckling load and more accurate results when using coarse

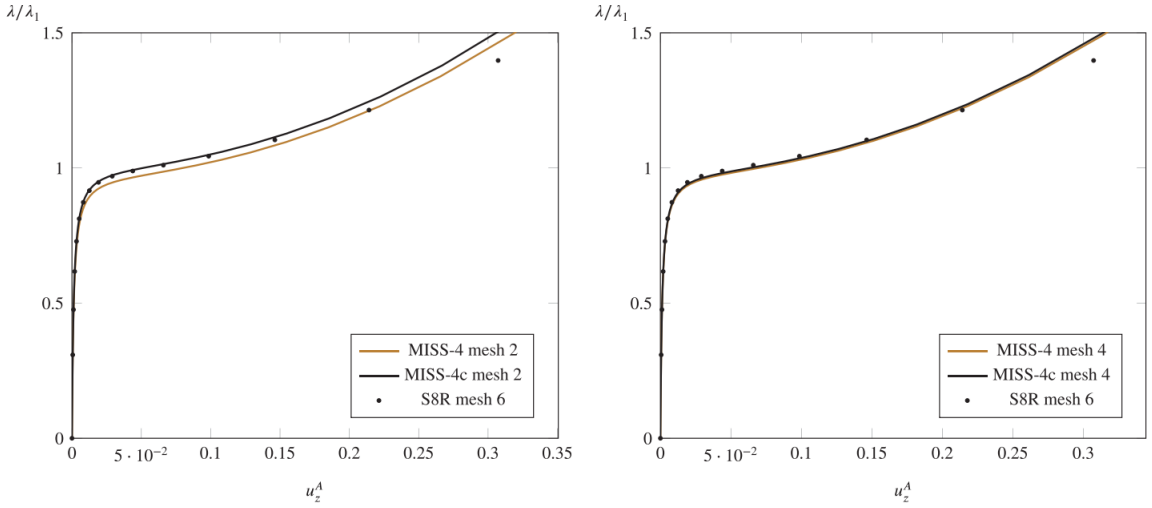

Figure 2: Composite laminated square plate: equilibrium paths. The vertical axis is normalised on the value of the lowest linear buckling load λ_1.

meshes than MISS-4.

Table 1: Composite laminated square plate: Four lowest buckling loads for different meshes.

mesh 2		mesh 3		mesh 4		S8R
MISS-4	MISS-4c	MISS-4	MISS-4c	MISS-4	MISS-4c	ABAQUS S8R
2.3295	2.3955	2.3348	2.3637	2.3535	2.3675	2.3841
3.2843	3.3634	3.1530	3.1819	3.13393	3.1470	3.1492
5.6080	5.7150	4.9946	5.0248	4.86214	4.8750	4.8393
9.5448	9.7231	7.7098	7.7431	7.31437	7.3273	7.2080

MISS-4C results to provide more accurate results than MISS-4 also in the evaluation of the initial postbuckling response of the plate obtained with the Koiter's analysis when using only the buckling mode corresponding to the lowest buckling load. This aspect is observed in Fig. 2 that shows the equilibrium paths evaluated using MISS-4, MISS-4C and compares them with that obtained with S8R and a path-following analysis in Abaqus.

4 CONCLUSIONS

This work presented some of the authors' developments in analysing lightweight composite laminated structures. The literature survey introduced a family of finite elements known as MISS elements, where MISS stands for mixed isostatic self-equilibrated stresses derived from the Hellinger-Reissner functional. Then, among the elements of the MISS family, emphasis was given to MISS-4C, a four-node element developed through the hybrid-Trefftz method so that its stress fields a priori satisfy both the equilibrium for zero bulk loads and the compatibility equations. As such, MISS-4C uses bespoke stress fields for studying composite laminated thin-walled structures with symmetric layups.Numerical results obtained for the initial postbuckling analysis of composite laminated plates under compressive loading showed that the element is robust and reproduces the equilibrium paths accurately also when using coarse meshes. Finally,

this work, together with a companion work presented in this conference [23], further proves that mixed FEs with an isostatic and self-equilibrated stress field provide higher accuracy and robustness than their corresponding mixed and displacement-based counterparts.

REFERENCES

[1] E. Barbero, A. Madeo, G. Zagari, R. Zinno, and G. Zucco. Imperfection sensitivity analysis of composite cylindrical shells using koiter's method. *International Journal for Computational Methods in Engineering Science and Mechanics*, 18(1):105–111, 2017.

[2] E.J. Barbero, A. Madeo, G. Zagari, R. Zinno, and G. Zucco. Koiter asymptotic analysis of folded laminated composite plates. *Composites Part B: Engineering*, 61:267 – 274, 2014.

[3] E.J. Barbero, A. Madeo, G. Zagari, R. Zinno, and G. Zucco. A mixed isostatic 24 dof element for static and buckling analysis of laminated folded plates. *Composite Structures*, 116:223 – 234, 2014.

[4] E.J. Barbero, A. Madeo, G. Zagari, R. Zinno, and G. Zucco. Imperfection sensitivity analysis of laminated folded plates. *Thin-Walled Structures*, 90:128 – 139, 2015.

[5] S. Cen, Y. Shang, C.-F. Li, and H.-G. Li. Hybrid displacement function element method: a simple hybrid-trefftz stress element method for analysis of mindlin–reissner plate. *International Journal for Numerical Methods in Engineering*, 98(3):203–234, 2014.

[6] K.-S. Chun, S.K. Kassegne, and B.K. Wondimu. Hybrid/mixed assumed stress element for anisotropic laminated elliptical and parabolic shells. *Finite Elements in Analysis and Design*, 45(11):766–781, 2009. cited By 9.

[7] Shahrzad Daghighi, Giovanni Zucco, Mohammad Rouhi, and Paul M. Weaver. Bend-free design of super ellipsoids of revolution composite pressure vessels. *Composite Structures*, 245:112283, 2020.

[8] Eisuke Kita and Norio Kamiya. Trefftz method: an overview. *Advances in Engineering Software*, 24(1):3 – 12, 1995.

[9] Tomasz Kubiak, Mariusz Urbaniak, Giovanni Zucco, and Antonio Madeo. Imperfection sensitivity analysis of the nonlinear stability of composite beams – numerical and experimental investigations. *Composites Part B: Engineering*, 94:360 – 369, 2016.

[10] F. S. Liguori, G. Zucco, and A. Madeo. A mixed hexahedral solid-shell finite element with self-equilibrated isostatic assumed stresses for geometrically nonlinear problems. *Accepted in International Journal for Numerical Methods in Engineering*, 2024.

[11] F. S. Liguori, G. Zucco, A. Madeo, G. Garcea, L. Leonetti, and P. M. Weaver. An isogeometric framework for the optimal design of variable stiffness shells undergoing large deformations. *International Journal of Solids and Structures*, 2020.

[12] F S. Liguori, G. Zucco, A. Madeo, D. Magisano, L. Leonetti, G. Garcea, and P. M. Weaver. Postbuckling optimisation of a variable angle tow composite wingbox using a multi-modal koiter approach. *Thin-Walled Structures*, 138:183–198, 2019.

[13] Francesco S. Liguori and Antonio Madeo. A corotational mixed flat shell finite element for the efficient geometrically nonlinear analysis of laminated composite structures. *International Journal for Numerical Methods in Engineering*, 122(17):4575–4608, 2021.

[14] A. Madeo, R.M.J. Groh, G. Zucco, P.M. Weaver, G. Zagari, and R. Zinno. Post-buckling analysis of variable-angle tow composite plates using Koiter's approach and the finite element method. *Thin-Walled Structures*, 110:1–13, 2017.

[15] A. Madeo, F. S. Liguori, G. Zucco, and S. Fiore. An efficient isostatic mixed shell element for coarse mesh solution. *International Journal for Numerical Methods in Engineering*, n/a(n/a).

[16] A. Madeo, G. Zagari, and R. Casciaro. An isostatic quadrilateral membrane finite element with drilling rotations and no spurious modes. *Finite Elements in Analysis and Design*, 50:21–32, 2012.

[17] A. Madeo, G. Zagari, R. Casciaro, and S. De Miranda. A mixed 4-node 3d plate element based on self-equilibrated isostatic stresses. *International Journal of Structural Stability and Dynamics*, 15(4), 2015.

[18] L. Magisano, D. Leonetti and G. Garcea. Koiter asymptotic analysis of multilayered composite structures using mixed solid-shell finite elements. *Composite Structures*, 154:296 – 308, 2016.

[19] Daniel Peeters, Daniel van Baalen, and Mostafa Abdallah. Combining topology and lamination parameter optimisation. *Structural and Multidisciplinary Optimization*, 52:105–120, 2015.

[20] K. Rah, W. Van Paepegem, A.M. Habraken, and J. Degrieck. A mixed solid-shell element for the analysis of laminated composites. *International Journal for Numerical Methods in Engineering*, 89(7):805–828, 2012. cited By 23.

[21] K.Y. Sze and L.Q. Yao. A hybrid stress ANS solid-shell element and its generalization for smart structure modelling. Part I - Solid-shell element formulation. *International Journal for Numerical Methods in Engineering*, 48(4):545–564, 2000.

[22] G. Zucco, R.M.J. Groh, A. Madeo, and P.M. Weaver. Mixed shell element for static and buckling analysis of variable angle tow composite plates. *Composite Structures*, 152:324 – 338, 2016.

[23] G. Zucco, F. S. Liguori, and A. Madeo. A hybrid hexahedral solid-shell element with self-equilibrated stresses for the geometrically nonlinear static analysis of composite laminated structures. *ECCOMAS, Lisbon, Portugal*, 2024.

[24] Giovanni Zucco and Paul M. Weaver. Post-buckling behaviour in variable stiffness cylindrical panels under compression loading with modal interaction effects. *International Journal of Solids and Structures*, 203:92 – 109, 2020.